The Effects of Varying Composition and Build Direction on Direct Metal Deposition Fabricated Inconel 718

A Senior Project

Presented to

The Faculty of the Materials Engineering Department

California Polytechnic State University, San Luis Obispo

In Partial Fulfillment

Of the Requirements for the Degree

Bachelor of Science

by

Jessica Fordham and Abigail Nilan

June 11, 2018

Abstract

Inconel 718 (IN718) is a popular wrought superalloy, and is currently being investigated for additive manufacturing (AM) applications in the aerospace industry. However, overaging and the presence of microcracks have caused a significant reduction in properties. The purpose of this study is to meet or exceed the mechanical properties of wrought IN718 by varying the composition and build direction of the AM alloy. Alternative compositions were selected with Oerlilon Metco's Rapid Alloy Development (RAD) software, and differ in niobium content, which increases the fraction of the primary strengthening phase (γ″). Direct metal deposition (DMD) was used to fabricate the samples, which then underwent a heat treatment to precipitate γ″. Tensile testing, metallography, and scanning electron microscopy (SEM) were performed on the samples. Tensile testing found that the AM samples could exceed wrought strength with the appropriate composition and build direction. The horizontal build containing the highest niobium percentage achieved an average yield strength of 1400 MPa, higher than the 1218 MPa for the wrought. Samples in the horizontal build direction were consistently stronger than vertical alternatives due to their anisotropic grain morphology. Despite comparable strength, AM samples of all compositions had significantly reduced ductility with an average range of 1-3% elongation compared to an average of 21% for the wrought samples. Microstructural analysis revealed dendritic structures and cracks between print layers in the AM samples, which contributed to this reduction in ductility.

Keywords: Inconel 718, Additive Manufacturing, Direct Metal Deposition, Superalloy, Materials Engineering, Rapid Alloy Development

Acknowledgements

The authors would like to thank Jonathon Bracci and Oerlikon Metco for sponsoring this project and facilitating the research. Additional thanks goes to Professor Blair London of the Materials Engineering Department who advised the team and supported the success of the project.

Table of Contents

List of Figures

List of Tables

1. Introduction

1.1 Problem Statement

Additive manufacturing (AM) is a rapidly developing field that is changing many different industries, including aerospace. For this technology to be adopted by this field, the material must comply with strict compositional and mechanical property constraints. Adequate research has not been conducted on the effect of new manufacturing techniques on traditional aerospace alloys. Literature in this field shows a potential for the use of additive manufacturing on nickel-based superalloy Inconel 718, but there are concerns regarding microstructural defects such as microcracking or overaging that would reduce mechanical properties. To address the problem, this project compared three alloy compositions of Inconel 718 produced in both vertical and horizontal build directions, to its traditional wrought form. The main goal of this research was to find the alloy composition and build direction that enhances mechanical properties, specifically yield strength, and elongation of Direct Metal Deposition (DMD) -built Inconel 718. These modified experimental factors should cause the AM-built Inconel 718 to meet or exceed the mechanical properties of its wrought alloy counterpart. The primary strengthening phase (γ'') fraction in Inconel 718 was increased by increasing niobium content in order to understand the limit before microcracking caused strength and ductility to decrease. Testing and analysis included tensile testing, metallography on the samples, and Scanning Electron Microscopy (SEM) fracture surface characterization. These tests allow for the comparison of mechanical properties, microstructure, and microcrack presence on AM and wrought samples.

1.2 Company Overview

This project is sponsored by Oerlikon Metco, formally Scoperta, located in San Diego, CA. Oerlikon Metco specializes in designing specialty alloys with its advanced modeling software, Rapid Alloy Development (RAD). RAD software sorts through a range of compositions to predict the ideal alloy for a specific application based on microstructure and specified properties. This method of alloy selection is cost effective and promotes innovation while keeping up with the strict material standards held by customers in the automotive, aviation, mining, oil and gas, health care, and agricultural industries. The RAD materials developed are used for various industry processes and products including thermal spraying, laser cladding, synchronizer coatings, aero engine coatings and hardbanding. Recently, Oerlikon Metco has been expanding to serve applications in additive manufacturing and aims to use its advanced computational software to model new powder alloys for this industry.[1]

1.3 Inconel 718

1.3.1 Inconel 718 Information

One of the prevalent high strength alloys used for aerospace applications is Inconel 718 (IN718). This is a nickel-iron based superalloy known for its ability to maintain strength and corrosion resistance under extreme environmental conditions, even close to its melting temperature. For IN718, this means it can be used at temperatures up to 760°C while resisting creep, fatigue, oxidation, and environmental degradation.[2]

1.3.2 Composition and Phases

The principal alloying element is nickel at 50-55 wt%, but there are also high concentrations of both chromium and iron at around 20 wt% each. The combination of alloying elements leads to a two phase equilibrium microstructure at room temperature made up of γ and γ' phases. A third, metastable phase known as γ″ is also present given specific processing conditions. Alloying elements added to the nickel base facilitate the development of the proper microstructure (Table I). Specifically, the 5.2 wt% niobium (Nb), promotes the formation of the γ″ phase. The iron in the Ni-based alloy primarily acts as a catalyst for the formation of γ″. Additionally, small amounts of aluminum and titanium are found on IN718, which contribute to the γ' phase. [3]

Table I: Chemical Compositions of IN718 Alloy Powders in wt% [2]

Alloy	Ni	Cr	Nb	Mo	Al	Ti	Fe	Si	Mn	C	S	O	N
IN718	50.7	19.6	5.21	3.21	0.59	0.98	19.4	0.13	0.10	0.04	0.01	0.04	0.02

1.3.3 Sample Compositions

In order to determine how the phase fraction of γ″ influences material properties, this study will look at three alloy compositions with varying amounts of Nb. Nb is an alloying element that acts to strengthen the metal by forming γ″. These alloys are designated as IN718, 718-X1, and 718-X2, where -X1 and -X2 have been modified from the standard IN718 such that -X1 has 6.62% Nb and -X2 has 8.52% Nb. By increasing the wt% Nb, the phase fraction of the metastable γ″ phase increases, as does the γ″ phase formation temperature. These values have been determined using Oerlikon's alloy modeling software (Table II).[1]

Table II: Composition, γ″ Formation Temperature, and Phase Fraction of Three Sample Alloys [1]

Alloy	wt% Nb	γ″ Formation Temperature	Phase Fraction of γ″ at 700°C
IN718	5.10	1,031°C	15.40%
718-X1	6.62	1,081°C	19.20%
718-X2	8.52	1,121°C	24.10%

1.3.4 Strengthening Mechanisms

The primary strengthening phase in IN718 is γ″, which forms precipitates to age harden the alloy. Metastable γ″ is an intermetallic compound composed of Ni_3Nb, that adopts the body-centered tetragonal (BCT) unit cell (Figure 1). This precipitate is coherent within the γ matrix, meaning the lattices are strained, but aligned between both phases. The γ matrix itself is a Ni-based solid solution in the face centered cubic (FCC) crystal structure.

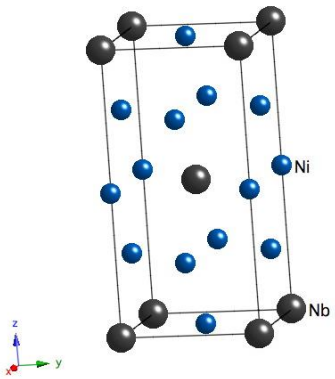

Figure 1: The unit cell of the γ″ phase, found in IN718. Body-centered tetragonal lattice of Ni and Nb atoms. Strengthening occurs by coherency strains and a low number of slip systems.[4]

Phases γ' and γ″ usually precipitate together, but γ″ is the principal strengthening phase due to high coherency strains in the lattice. The γ phase serves as the matrix in which γ″ precipitates. The two phases have similar lattice parameters, meaning γ″ phase precipitates to be oriented parallel to the γ lattice. When the precipitates are small, this results in a coherent phase interface which strains the lattice and makes it difficult for dislocations to travel through. Additionally, γ″ is an intermetallic compound with an ordered crystal structure which increases the alloy strength. The distinct chemical formula of each precipitate means movement of dislocations through this phase would disrupt the composition at an atomic level. Resistance to this dislocation motion is another strengthening mechanisms of IN718.

1.3.5 Post-Processing Heat Treatment

The proper precipitate microstructure is achieved due to solutionizing followed by one or more precipitation aging heat treatments. Specifics of this treatment vary depending on the application, and the γ″ phase formation temperature which may be altered due to compositional changes from the standard IN718. The supersaturated γ matrix is first established by solutionizing the part at high temperatures between 925 to 1200°C. The alloy is held at this elevated temperature for 1 to 2 hours to completely dissolve the aging constituents in solution, then returned to room temperature by air or water quenching. If the material is not properly solutionized prior to aging, the desired microstructure and mechanical properties will not be achieved. The solutionized material should be a single γ phase meaning it has a homogeneous structure and chemical

composition. Any secondary phase would disrupt the spontaneous nucleation of precipitates during aging, and reduce the strength of the alloy. After quenching, the material is double annealed, first at a high temperature, and then at a lower temperature. [5]

The high temperature anneal promotes the rapid nucleation of dispersed precipitates. By adding heat to the system, the higher temperature increases the rate of diffusion, prompting γ″ phase to nucleate. Next, the temperature is reduced and diffusion is slowed. The second annealing takes place at a lower temperature to encourage grain growth, instead of new precipitate nucleation. Proper solutionizing and annealing temperatures were confirmed using the time-transformation-temperature diagram for IN718 (Figure 2). An example annealing treatment would take a total of 18 hours: After solutionizing at 1100°C and quenching, the IN718 part would be placed in a furnace at 720°C, and held for 8 hours. The furnace temperature would then be reduced to and held at 620°C for an additional 10 hours. This aging yields a fully γ″-strengthened part. [5,6]

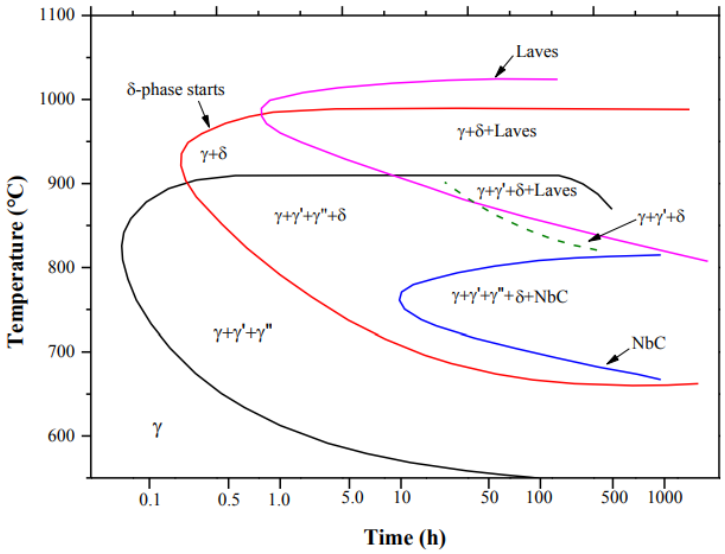

Figure 2: Time-transformation-temperature diagram of IN718 alloy system. Diagram was adapted from the American Welding Society.[7]

Proper heat treatment procedures are needed to ensure the γ″ phase does not overage to produce the stable orthorhombic δ phase. This phase is incoherent within the lattice, and does not offer strength when present in large quantities. The δ phase forms in temperature ranges of 650-980°C, and nucleates at γ grain boundaries at the expense of the γ″ phase. At temperatures closer to 700°C, δ formation is accompanied by the rapid coarsening of γ″. Above, 885°C, γ″ is no longer stable and plates of δ form rapidly. Sometimes this δ distribution can work to control and refine grain size, but more often extensive amounts of the phase will lower tensile properties (Table III).[8]

Table III: Ultimate Tensile Strength of Wrought IN718 as a Function of Heat Treating Temperature [5]

Solution Heat Treatment	UTS (MPa)
None (direct aged)	1525
940°C, 1 h	1460
955°C, 1 h	1420
970°C, 1 h	1405
1010°C, 1 h	1390

As shown above, the higher temperature heat treatments cause the alloys Ultimate Tensile Strength (UTS) to decrease. This is because of the extensive amount of δ phase that forms at high temperatures. High temperature exposure can also promote the formation of undesirable secondary phases such as σ and Laves. Laves is a hexagonal phase that forms elongated platelets at high temperatures. The σ phase is tetragonaly packed and forms irregularly shaped globules after extended exposure between 540 and 980°C. Due to their morphology, low ductility, and tendency to tie up hardening elements, these secondary phases lead to property degradation, reducing alloy effectiveness.[9]

1.3.6 Mechanical Properties and Microstructure of IN718

Proper processing and heat treatment of IN718 yield an alloy with desirable mechanical properties. These mechanical properties derive from the γ″ precipitation-hardened microstructure. Typically, IN718 undergoes wrought processing, so additive manufacturing introduces new variables that need to be further explored.

In its wrought form, IN718 typically exhibits three intermetallic precipitate phases: γ′, γ″, and δ. The metastable phases responsible for strengthening are γ′ and γ″, whereas δ is an undesirable phase that results from overaging. Each precipitate phase takes on a unique shape in the matrix. γ′ precipitates are cuboidal or spherical, while γ″ precipitates are lenticular and disc-shaped (oblate spheroid) (Figure 3).[10] The lenticular γ″ phase acts as the primary strengthening phase by forming coherent precipitates that are densely packed in arrays aligned parallel to slip planes. These coherent precipitates cause distortion within the γ lattice and induce strain which adds an extra barrier for dislocation movement, increasing the strength of the material. The cuboidal γ′ phase has a similar lattice parameter to the matrix, thus forming coherent precipitates.[11] Similar to γ″ mechanism, dislocation movement is difficult, which further strengthens the alloy.

Figure 3: Transmission electron micrograph (3000X) of the γ' and γ" phases of wrought IN718 after 760°C anneal.[10]

1.4 Additive Manufacturing

Additive manufacturing (AM) is a rapidly developing field that is changing many different industries. Various technologies have made AM a reality for a wide range of materials from thermoplastic polymers to ceramics to metals. For certain applications, AM has clear advantages compared to traditional manufacturing methods such as casting and wrought-processing. These advantages include the ability to enhance rapid prototyping, reduce waste, and manufacture complex parts.[12]

One industry in which AM has the potential to have a significant impact is in aerospace. From engine parts to cabin interiors, the industry is turning to AM to increase performance and reduce costs of their products. The AM technique examined specifically for this project is Direct Metal Deposition (DMD). This is an attractive option for fabrication of complex-shaped, high strength metallic components. These can be difficult to produce by conventional manufacturing processes due to shaping restrictions and limitations as well as the cost of small batch sizes. [13]

The materials used in aviation must undergo a unique set of environmental stressors, which has led to the development of specific alloys to meet those performance needs. For example, nickel-based superalloys are a class of alloy that can serve at temperatures above 700°C for an extended period of time without significant deterioration in mechanical properties. These alloys are ideal for engine parts, which can be complex and better-produced by AM. DMD-produced parts made from the nickel-based superalloy IN718 are examined in this study. IN718 is a high-temperature alloy and is broadly used in the aerospace industry due to its superior mechanical properties and oxidation resistance at elevated temperatures, which makes the alloy ideal for aerospace engines and gas turbines.[15]

1.4.1 Direct Metal Deposition

Direct Metal Deposition (DMD) is a type of additive manufacturing technique under Laser Metal Deposition (LMD). The LMD technique also includes light engineered net shaping (LENS) and direct light fabrication (DLF) processes. DMD produces fully dense, functional metal parts by depositing metal powders using laser melting and a patented closed-loop control system to maintain dimensional accuracy and part integrity. The closed-loop control system differentiates DMD from LENS and DLF processes, which allows the system to adapt to controlled composition and microstructure. This process varies from Selective Laser Melting (SLM) in that the powder feeder and laser system are located in the same coaxial nozzle system (Figure 4). In the SLM method, the laser and metal powder are located in separate parts of the machine, and the powder forms a bed for the laser to sinter.[16]

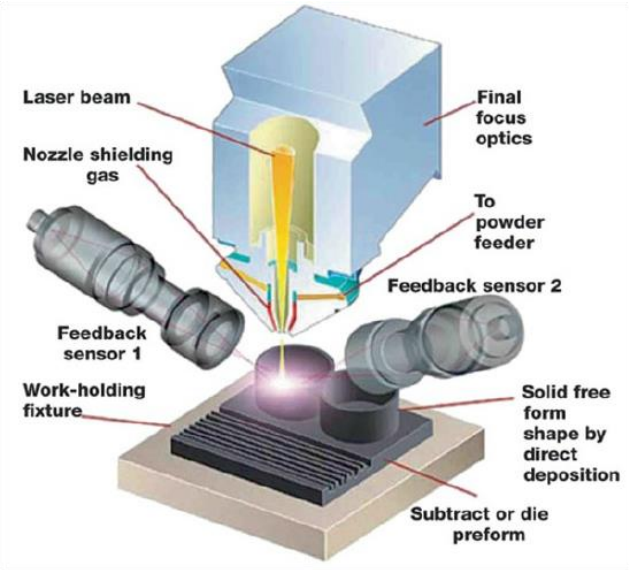

Figure 4: DMD process schematic shows coaxial nozzle feeding powder metal into laser path to build up a part.[12]

DMD uses a Laser Aided Manufacturing (LAM) process which focuses a high energy laser beam onto a substrate or a previously deposited layer, producing a melt pool into which a small amount of powder metal is injected. Metal powders are simultaneously delivered into the melt pool by a specially designed coaxial nozzle (Figure 4). DMD ″blows″ powder out of the coaxial nozzle and the laser melts the material. The nozzle is designed such that the powder streams converge at the same point on the focused laser beam. A computer numerical control (CNC) system is used to simultaneously control the nozzle and the beam focusing optics according to a tool path generated from a computer-aided design (CAD) model. Thus, a three-dimensional object is formed layer by layer.

DMD systems are equipped with a three or five-axis head and a rotary axis on the work table that can allow deposition at almost any angle, further adding to the complex geometry capabilities of

DMD. Additionally, recent advances in sensor technology have shown that the closed-loop control system can be temperature-controlled. Closed-loop control systems act as an optical feedback sensor that can control the melt pool during real time.[4] This controlled heat-input feature of DMD results in minimal heat affected zones (HAZ) and allows parts to be built with desired microstructures and mechanical properties. [12]

Inert gas is blown through the nozzle to help both in powder delivery and shielding the deposit from oxidation. Shielding is a way to seal the build chamber and produce adequate pressure to drive away the ambient air. A separate carrier gas is blown through the powder feed channels to assist in powder delivery to the nozzle. This carrier gas is often a mixture of argon and helium. A side injection nozzle can build up volume rapidly whereas the concentric nozzle can provide better resolution. In an ideal system a rotating head with both nozzles should be available.[16]

1.5 Challenges with AM

1.5.1 Build Direction Effects on Microstructure

The AM process involves a layer-by-layer manufacturing approach which introduces rapid thermal gradients. The successive stage of heat conduction from the molten zone and fast solidification facilitate the growth of columnar dendritic grains parallel to the build direction in the as-deposited alloy.[17] As samples are built, dendrites advance through epitaxial growth while each new layer fuses with the partially melted layer below it.[11] This results in a microstructure made up of transcending dendritic layers.

An important feature of AM is the occurrence of direct solidification (DS). DS occurs when the melt solidifies in a single direction, resulting in a highly anisotropic structure in the as-deposited solid. In IN718, the primary dendrite arms grow along the build direction which forms columnar structures. The formation of the dendrites during the solidification process is caused by the undercooled liquid metal. The undercooled liquid initially causes the formation of solid nuclei in the melt which keep growing during solidification. At some point, the anisotropy in the surface of the solid-liquid interface leads to a preferred growth due to the attempt of the solid to minimize its surface energy. The minimization normally takes place at the tips of the dendrites with the highest specific surface energy, which subsequently leads to the growth of the columnar structures.[18]

This DS effect was observed in multiple studies which provide insight into how the microstructural morphology of Ni-based superalloys changes with AM. One study looked at DMD-produced IN625, a precipitation hardened superalloy similar to IN718. As deposited, the microstructure consisted of columnar dendrites that grew epitaxially from the substrate (Figure 5a). There were no visible cracks or solidification error porosities which resulted in high hardness for the fine, supersaturated microstructure.[17] Similarly, a study on IN718 produced by SLM revealed columnar grains oriented parallel to the build direction (Figure 5b).[14] SLM differs from DMD processing, but both techniques rely in the heating of individual melt pools from

which grains solidify. For IN718, these oriented columnar grains are composed of γ″ and contain many densely packed incoherent precipitates.

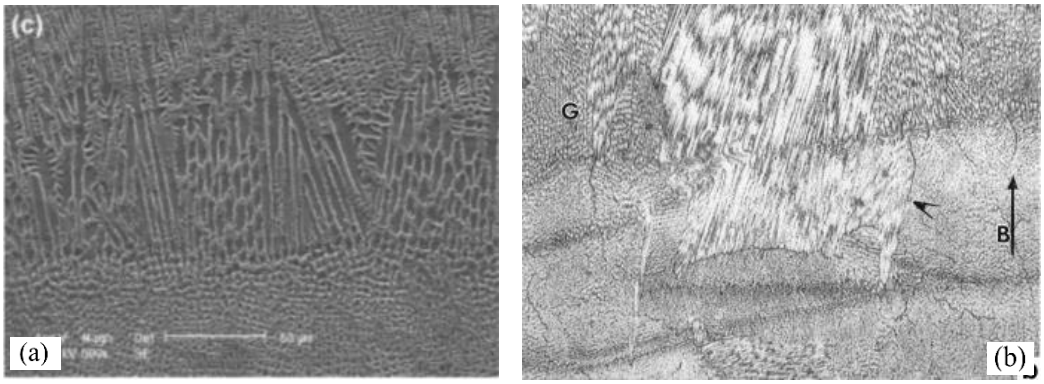

Figure 5: Columnar dendrites form parallel to build direction for (a) DMD-produced IN625 and (b) SLM-produced IN718. The dendritic columns of γ″ form from melt pools.

1.5.2 Microcracking

One common problem that has been encountered using AM processes on Ni-based superalloys is microcracking. Microcracking can cause a significant reduction in mechanical properties because of the resulting porosity and residual stresses. The mechanisms for the thermal residual stress that arises from AM include the Thermal Gradient Mechanism (TGM) and the cool-down phase of the molten top layers.[14] The TGM causes compressive strains between the layers of the AM part. The rapid heating of the top surface from the fusion of the metallic powder to the part, along with the slow heat conduction of the material forms a steep temperature gradient between the two layers. Compressive strains are formed when the molten outer layer expands and is restricted by the cooler lower layer. Additionally, as the top layer solidifies, it shrinks due to thermal contraction and induces a bending angle towards the laser source and produces a tensile stress in the build direction. As the layers build on top of each other, a series of compressive and tensile stresses result throughout the part.

Both of these mechanisms can lead to stress relief by cracking when stresses build up in the part and exceed the UTS. At solid surfaces, this fracturing is referred to as hot cracking. Research has considered that crack susceptibility (χ) be considered to determine the processability of the alloy.[19] χ relates to ultimate tensile strength (σ_{UTS}) and thermal stress (σ_T) in the material (Eq. 1).

$$\chi = \frac{\sigma_{UTS}}{\sigma_T} \qquad \text{(Eq. 1)}$$

Thermal stress is dependent on the specific heat capacity of the material, along with its thermal expansion coefficient. For a material to withstand hot cracking, the UTS needs to be greater than thermal stress (χ>1), as shown in Eq. 1. Because microcracking tends to be the cause of the most

detrimental mechanical property effects of Ni-based superalloys, a goal to increase χ will be the main focus of this study. Thermal stress remains for the most part unchanged, so improving the UTS of the alloy is a primary concern. To do this, the composition of IN718 can be manipulated to achieve a desired microstructure similar to the wrought alloy.

One method developed to eliminate cracks is known as hot isotrostatic pressing (HIP). HIP is a post-treatment that uses heat and pressure to heal defects and densify the material without changing the shape.[18] Cracks are eliminated through grain boundary movement and diffusion-controlled creep, which optimizes the material's microstructure. This treatment has also been shown to improve mechanical properties such as hardness, strength, toughness and shock resistance.

1.5.3 Other Challenges

Grain size varies depending on the print location within the part. A higher temperature gradient results in a smaller grain size because the alloy cools more rapidly and there is a larger driving force for grain nucleation. In sections that are taken close to the bottom of the part, heat dissipates through the substrate, cools rapidly, and produces finer grains. Contrarily, sections taken from the middle of the part reveal coarser grains because the surrounding material has a higher temperature when each layer is deposited, and thus had a smaller temperature gradient.[19] This phenomena is illustrated in SLM-printed IN718, showing the melt pool morphology near the substrate layers and on the top deposited layers (Figure 6).

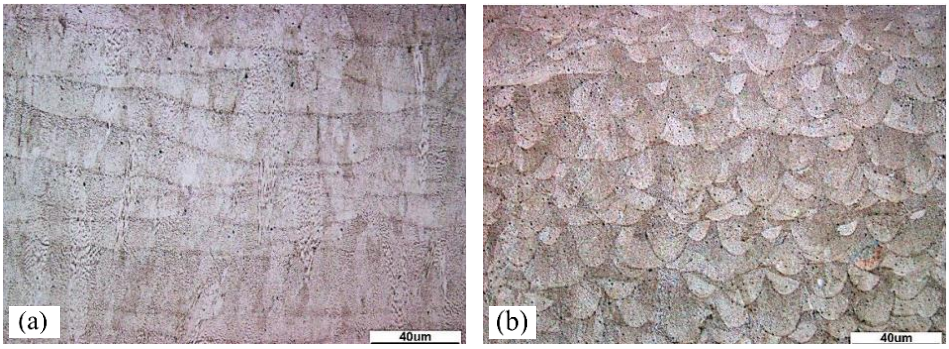

Figure 6: Melt pool morphology with reference to SLM-printed IN718 for (a) near the top and (b) near substrate deposited layers.[7]

Additionally, the alloy's crack susceptibility can depend on processing parameters. Experimentation has been performed in which processing parameters were varied to observe cracking behavior in Ni-based superalloy Rene 104 produced by direct metal fabrication. Micrographs were examined and analyzed with an image processing software to measure the lengths and counts of the cracks in each sample. These studies found that crack formation closely depends on the heat input.[17] This conclusion is based on the fact that no cracks were present in thin-walled samples, but cracks were found in cuboid samples. The thin-walled samples were

produced with a single pass of the laser, whereas cuboid samples were produced with a multi-pass which generated a higher thermal gradient within the material.[20]

Additionally, studies found that certain locations are more susceptible to crack formation. Cracks form when a high strain energy within the microstructure causes internal stress. Cracks are most likely to initiate at grain boundaries because they store interfacial energy and are strained. While grain boundaries are the favorable site, some cracks also form at pores within the material. The rapid cooling rates present during DMD have an effect on the material's microstructure. Experimentation indicated that a temperature gradient of 200~500 K/mm, and a small molten pool of around 3.14mm^2 yielded fine, directional dendrites. These dendrites grew epitaxially along the deposition direction and had a columnar structure.[20]

The laser's level of heat input, which can be evaluated by looking at the laser energy density, is another variable that affects crack formation. The energy density is a function of laser power, hatch spacing, slice thickness, and scanning velocity. Studies found that the cracking sensitivity increases as the volume energy density increases. This supports the trend that high temperature gradients are more susceptible to crack formation.[17]

A main component of this project is comparing the tensile properties of DMD-processed IN718 to its wrought-processed counterpart. There is limited research on the specific properties of DMD-produced IN718, but data was found for the superalloy manufactured by SLM. Although SLM will not be used for this study, the two AM techniques produced similar precipitate structures (Figure 5). When mechanically compared, it was found that SLM and wrought-manufactured IN718 have similar properties across both processing's annealed samples (Table IV). The yield and UTS of SLM IN718 slightly exceed the wrought/annealed sample, while the elongation is essentially the same. When aged, the wrought strength (yield and UTS) exceeded the SLM-processed sample, but the elongation was significantly reduced. Altering the composition of the alloy and controlling the heat treatment shows promise in optimizing the mechanical properties of IN718 after DMD fabrication.

Table IV: Mechanical Properties of IN718 After SLM and Wrought Processing[14]

Tensile Orientation and Processing Condition	Hardness (HRC)	0.2% Yield strength (Gpa)	UTS (GPa)	% Elongation
x-axis, SLM, HIP + annealed	34	0.89	1.20	28
wrought (annealed)	24	0.83	1.10	31
wrought (aged)	45	1.40	1.60	16

These wrought properties, along with tensile test experimental data and microstructural analysis will be compared to varying compositions of IN718 fabricated with DMD. The goal is to identify

an AM alloy that meets or exceeds the mechanical properties of wrought IN718 for use in aerospace applications.

2. Experimental Procedure

This project focused on comparing the mechanical properties and microstructures of varying AM samples to traditional wrought IN718. For this reason, composition and build direction were varied, while other factors such as aging treatment and print parameters were kept constant.

2.1 Composition

Using Oerlikon's RAD software, two alternative alloys were identified to compare to IN718. These compositions were designated X1 and X2 and differed from IN718 in increasing Nb content (Table V). Nb promotes the formation of the γ" phase, which is the primary strengthening phase in the alloy.

Table V: Alloy Compositions (in wt%) Generated by RAD Software[1]

Alloy	Al	C	Co	Cr	Fe	Mn	Mo	**Nb**	Ni	Si	Ti
IN718	0.45	0.05	0.06	18.88	17.88	0.06	3.06	**5.10**	53.50	0.04	0.92
X1	0.44	0.05	0.06	18.58	17.59	0.06	3.01	**6.62**	52.64	0.04	0.91
X2	0.43	0.05	0.06	18.20	17.24	0.06	2.95	**8.52**	51.57	0.04	0.89

2.2 Build Direction

The three compositions were fabricated in both the horizontal and vertical build directions. Each build direction consisted of DMD print layers that were built up from the substrate surface in the z-axis for final dimensions of 4 mm x 50 mm x 410 mm. Argon was used as the shielding gas in which an 800 W laser moved at a 1300 mm/min scan rate to build up layer thickness of 0.11 mm. The powder was ejected at a 3 g/min feed rate into the laser's 2.9 mm spot diameter. These print parameters were kept constant across composition. Tensile coupons were wire electrical discharge machined (EDM) such that loading axis ran parallel to print layers for the horizontal build, and perpendicular to print layers for the vertical build (Figure 7).

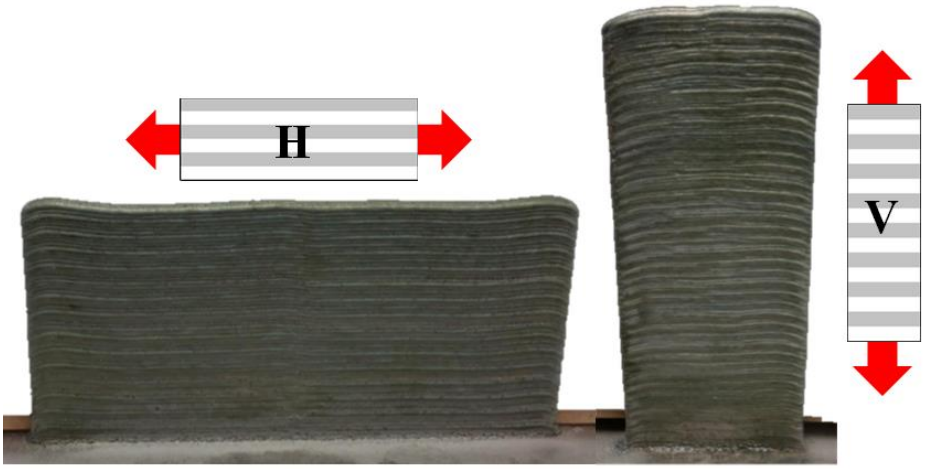

Figure 7: Samples were fabricated by DMD in the vertical and horizontal build directions. The red arrows indicate the specified tensile loading direction.[1]

2.3 Heat Treatment

Each composition and build direction underwent a solutionizing and aging heat treatment in order to get the desired precipitation hardened microstructure. The solutionizing heat treatment differed for each composition, based the γ" formation temperature which was identified using Oerlikon's RAD software (Table VI). After solutionizing, the samples were water quenched. Aging time and temperature were kept constant across all samples at 718°C for 8 hours, followed by 8 hours at 621°C.

Table VI: Solutionizing and Aging Heat Treatments[1]

Alloy	Solutionizing Temp. and Time	Aging Temp. and Time
IN718	1062°C/1 hour	• 718°C/8 hours • 621°C/8 hours
X1	1112°C/1 hour	
X2	1152°C/1 hour	

2.4 Testing

2.4.1 Tensile Testing

Sample mechanical properties were obtained by tensile testing. Three tensile coupons were machined using wire EDM from each composition and build direction combination, resulting in 21 total samples (Figure 8). The bars were tested following ASTM Standard E8 / E8M- 16a.[21] Once sample bars were aligned vertically into the Instron tensile testing machine, an extensometer was placed within the gauge length. As testing proceeded, the extensometer was removed once the sample had extended to 0.9% elongation. The data collection within a sample

group was staggered to maximize consistent testing across each sample set. The specific mechanical properties that were examined in this study were yield strength and percent elongation.

Figure 8: Image of tested tensile coupons of sample X1 in the horizontal build direction.

2.4.2 Metallography

Microstructural features were revealed for the wrought and horizontally built AM samples by performing metallography. Sections were cut from the tensile bar and mounted in Bakelite such that the wide "face" of the tensile bar faced outward at the mount surface. This surface was ground up to 1200 grit grinding paper, then polished up to a 1 µm polishing grit using a diamond suspension. Optical microscopy qualified the samples as nearly scratch-free and ready for etching.

Kalling's Reagent was chosen as the etchant because of its corrosive ability for nickel iron based superalloys such as IN718. This etchant consists of 50 mL hydrochloric acid (HCl), 2.5 g cupric chloride ($CuCl_2$), and 50 mL ethanol (C_2H_6O). Reagents were combined in the fume hood. Samples were then submerged in the etchant for around 60 seconds, then rinsed in water and dried.

After the proper etching time had been reached, the microstructures were examined under optical microscopes. Representative images were captured for each sample. These images were oriented such that the tensile loading axis ran horizontally across the image.

2.4.2.1 Safety

Metallography was conducted using proper safety protocol. An SOP was developed for the etching procedure (Appendix I). Safety Data Sheets for all chemicals used were referenced when composing the SOP. [22, 23, 24]

2.4.3 Scanning Electron Microscopy

The fracture surfaces of the AM samples were examined under the SEM to further understand the reasons for the low ductility. Sample X2 built in the horizontal direction and X1 build in the vertical direction were analyzed to see possible variances between composition and build direction. First, the fracture surface samples were cut from the tensile bar using an abrasive cut-off saw. To clean the surface, each sample was immersed in ethanol and ultrasonicated for 5 minutes.

The samples were mounted and imaged using a FEI-Philips Quanta 200 ESEM. The parameters included a 20 kV accelerating voltage in high vacuum mode and a spot size of four. Magnifications of 150X-1000X were used to produce ideal images of the fracture surfaces.

3. Results

3.1 Tensile Testing

The tensile testing data shows that the AM samples had consistent stress-strain behavior between the three samples (Appendix II, III, IV). The X2 samples exhibited an elastic region of deformation up until a percent elongation of 0.8% (Figure 9). After yield, the samples underwent a plastic region up until a percent elongation of 1.9% to 2.4%. This shows the samples still underwent some plastic deformation before fracture.

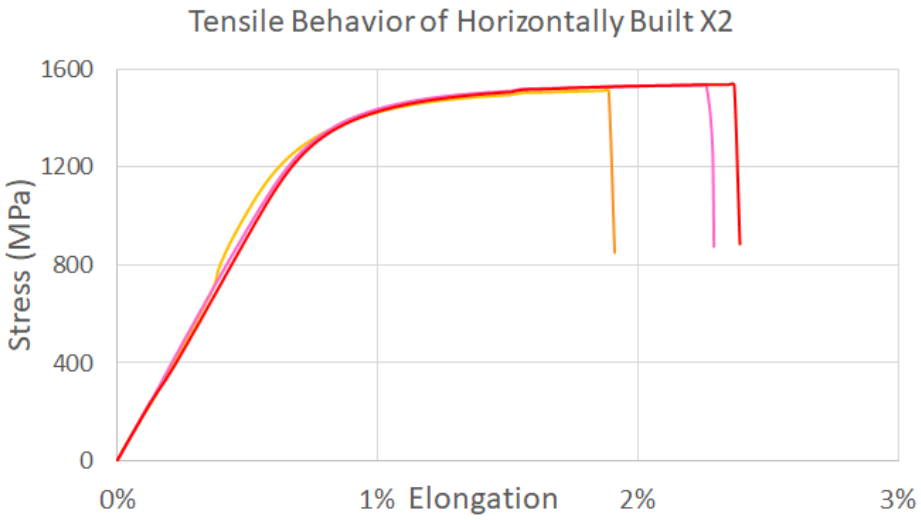

Figure 9: Stress-strain curve of X2 samples built in the horizontal direction.

The percent elongation results for the samples showed that the wrought samples had significantly higher percent elongation than the AM samples (Figure 10). The wrought samples had an average percent elongation of 21% compared to the AM samples, which had an average percent elongation between 1-9%. The IN718 samples built in the vertical build direction had a larger average ductility than the other AM samples. Possible reasons will be discussed throughout this report.

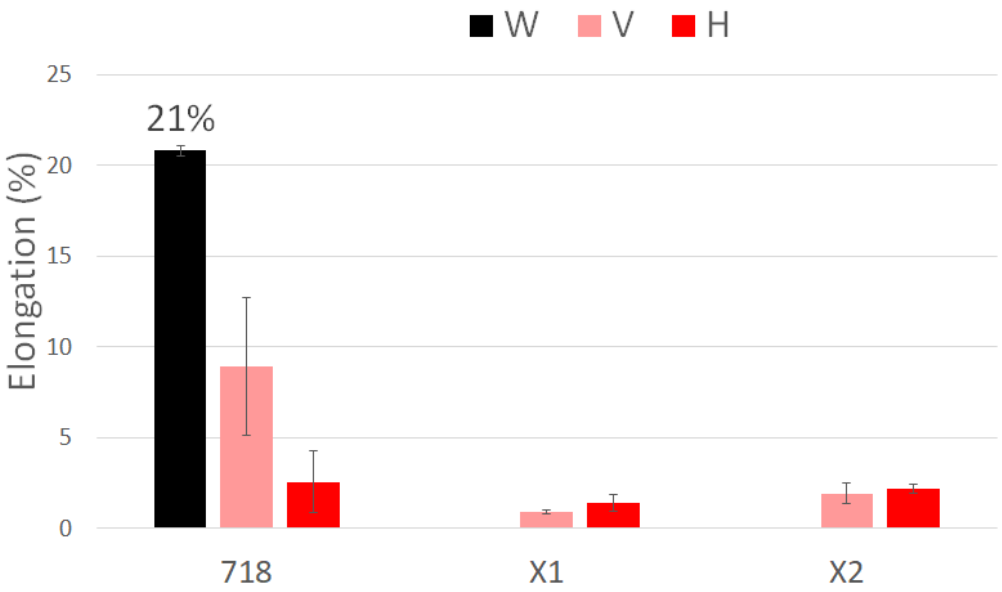

Figure 10: Average percent elongation and standard deviation results of samples tested. W, H, and V labels represent wrought, horizontally built AM, and vertically built AM processing.

The yield strength results showed more promise in exceeding the wrought strength. The wrought samples had an average yield strength of 1218 MPa (Figure 11). Each composition increased in yield strength as the Nb composition increased, which was expected because Nb promotes the formation of the γ″ strengthening phase. The X2 composition was able to exceed the wrought yield strength in both the horizontal and vertical build directions. Lastly, all compositions built in the horizontal build direction had consistently higher average yield strengths.

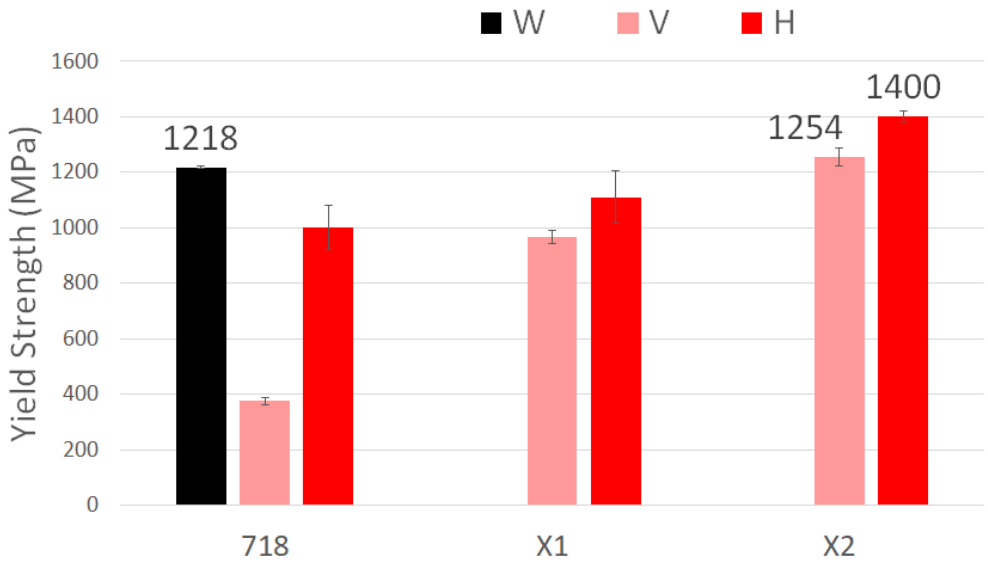

Figure 11: Average yield strength and standard deviation results of samples tested.

3.2 Metallography

The wrought microstructures showed some large grains, as well as twinning in many of the grains (Figure 12). The porosity shown was likely due to inconsistencies from polishing since wrought processing treatment should produce a fully dense part.

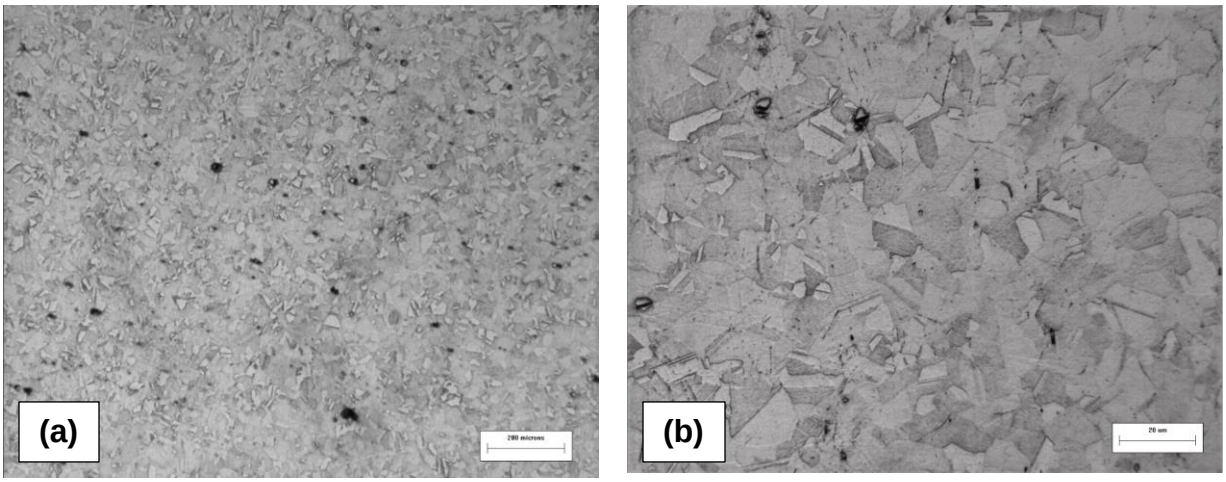

Figure 12: Microstructural images of wrought IN718 at 50X (a) and 200X (b).

The additive manufactured microstructures revealed stark contrasts from the wrought samples. After etching, the grains were clearly not visible and dendritic structures formed in the IN718 AM samples (Figure 13). These dendritic structures were likely a secondary σ phase. The γ′′ precipitates were also not seen optically, which signifies these precipitates were too small to be seen in a standard microscope. Likely a Transmission Electron Microscope (TEM) was needed to see these precipitates. Distinct layers that were expected to be seen in these microstructures were

also not observed in the AM samples. Cracks were visible in the IN718 AM samples, and seemed to propagate in a random manner.

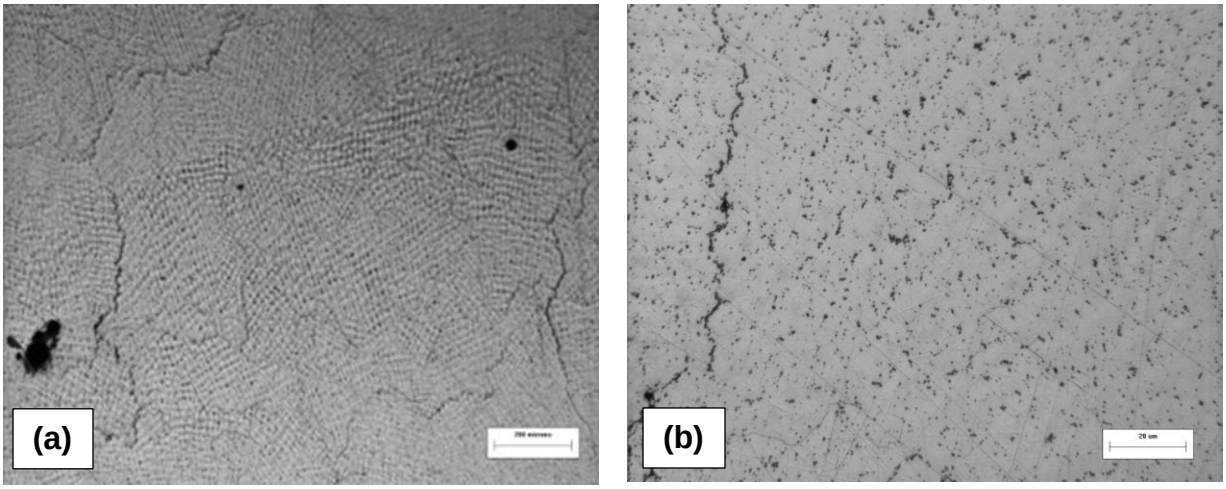

Figure 13: Microstructural images of IN718 built in the horizontal direction at 50X (a) and 200X (b).

Similarly, cracks and dendritic structures were visible in the horizontal build direction of X1 (Figure 14). In this modified composition, the cracks are larger than in the IN718 AM samples, and there appears to be less dendrites than found in the IN718 samples built in the horizontal direction. The cracks shown seem to align along the layers of the sample, which leads us to believe thermal stresses caused the cracking in the sample.

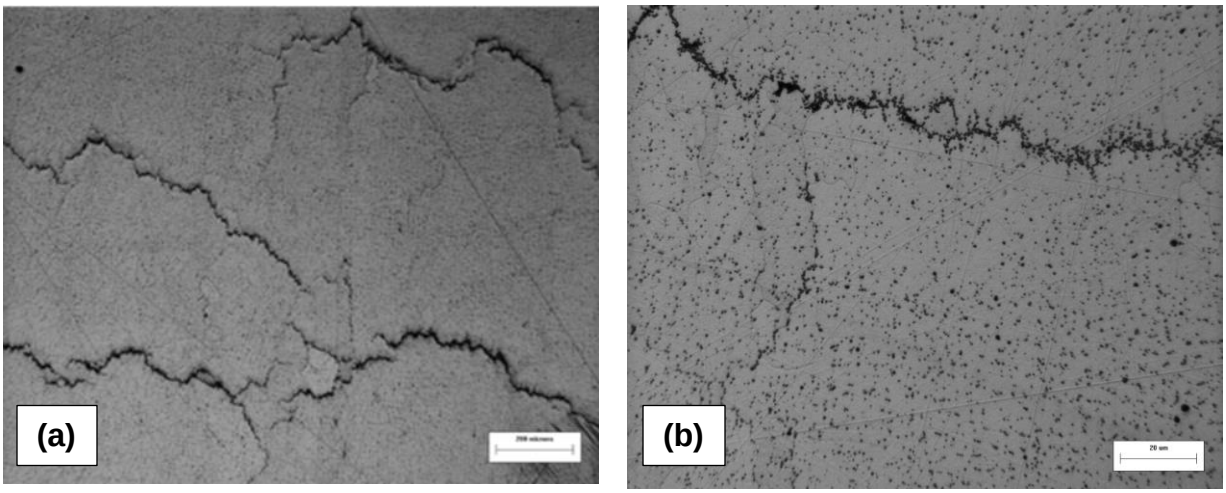

Figure 14: Microstructural images of wrought X1 built in the horizontal direction at 50X (a) and 200X (b).

The microstructure of X2 built in the horizontal build direction showed similar dendritic growth and less cracking as in the other additive manufactured samples (Figure 15). This could be because X2 had the most γ'' phase amount, and was able to resist thermal stresses caused from AM. Grain growth was more apparent in this sample than in the other additive manufactured samples as well.

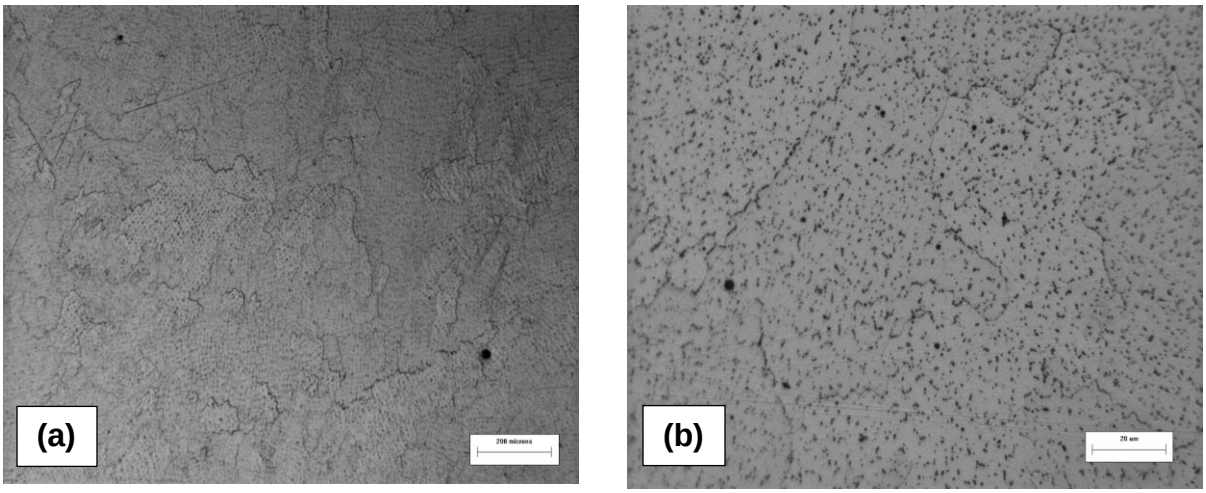

Figure 15: Microstructural images of wrought X2 built in the horizontal direction at 50X (a) and 200X (b).

3.3 Scanning Electron Microscopy

Using the SEM, the tensile sample fracture surfaces were first analyzed at 150X magnification to see large areas of the fracture surface (Figure 16). Compositions X2 and X1 were imaged to understand the low ductility present in the AM samples. At low magnification, the γ″ precipitates were not visible, as expected. The layers fabricated during direct metal deposition were easily seen as well as cracks in 718X2_H_2 (Figure 16, a).

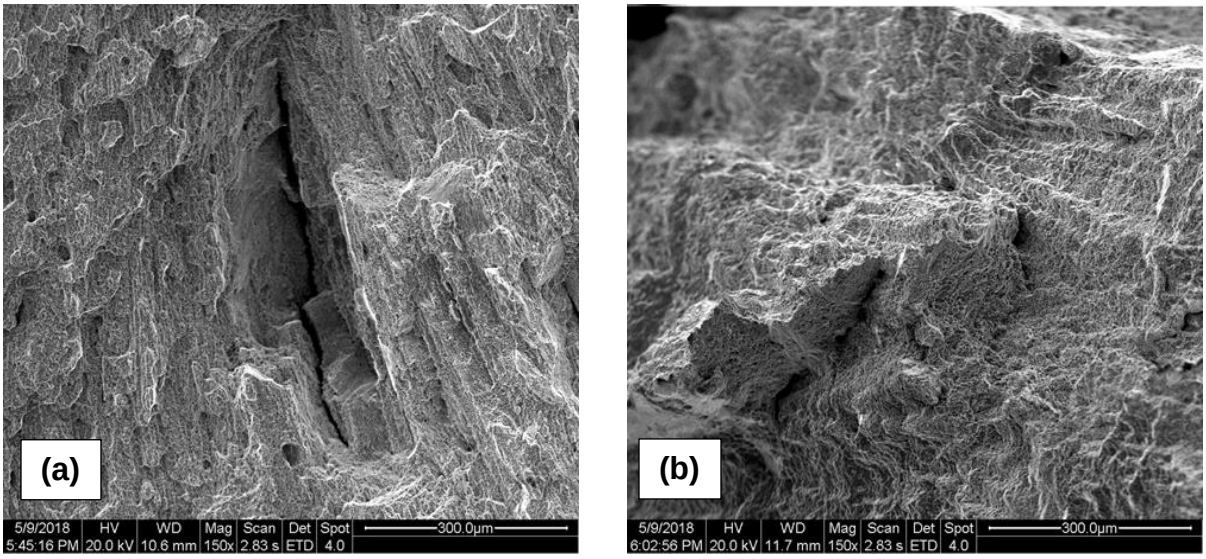

Figure 16: SEM images of 718X2_H_2 (a) and 718X1_V_1 (b) at 150X.

At higher magnification, the presence of microvoids indicated a ductile fracture on the surface of the samples of both compositions (Figure 17). The images showed no significant differences between the samples built in the horizontal and vertical build directions. The microvoids were about 5 μm in diameter for both samples imaged. It was concluded that the failure mechanism present in all AM samples was microvoid coalescence. This mechanism will be discussed further

later in this report.

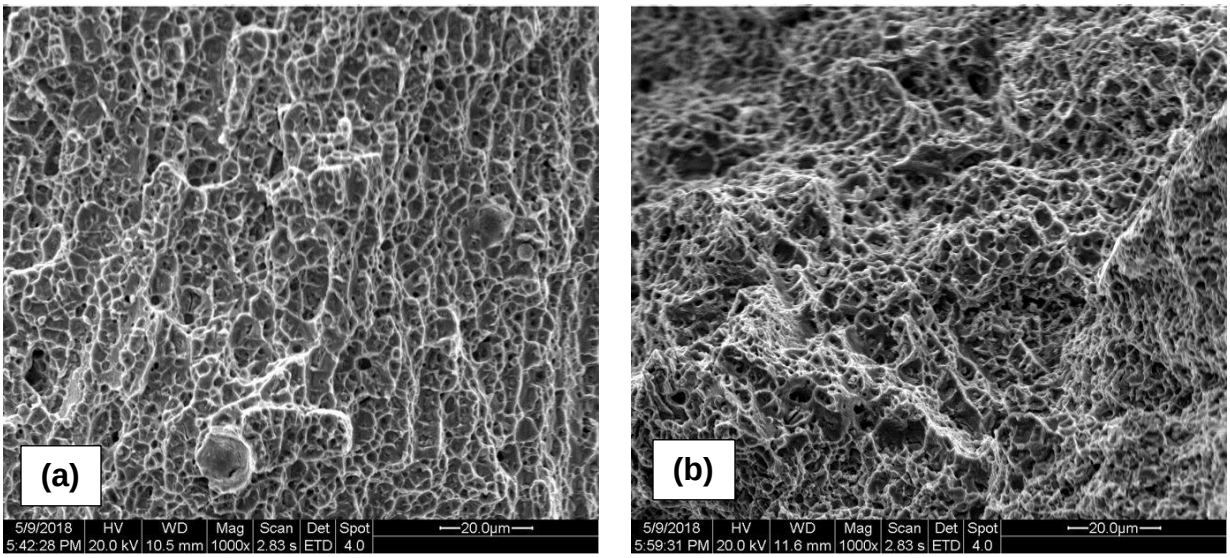

Figure 17: SEM images of 718X2_H_2 (a) and 718X1_V_1 (b) at 1000X.

4. Discussion

4.1 Low Percent Elongation

Tensile test results show that the wrought IN718 samples had an average percent elongation of 21% while the AM samples had a percent elongation between 1-9%. Possible reasons for this low ductility were examined.

4.1.1 Microcracking

One reason for the low ductility may be the presence microcracks which formed during DMD. Stresses are localized at the crack site, and plastic deformation is inhibited. Additive manufactured IN718 is known to be susceptible to cracking due to a variety of mechanisms that depend on crack location. In the top layer of the deposit, solidification cracks occur due to the high thermal gradient present. Cracks form in the underlying layers, which are in the heat affected zone, due to constitutional liquation (Figure 18).[21]

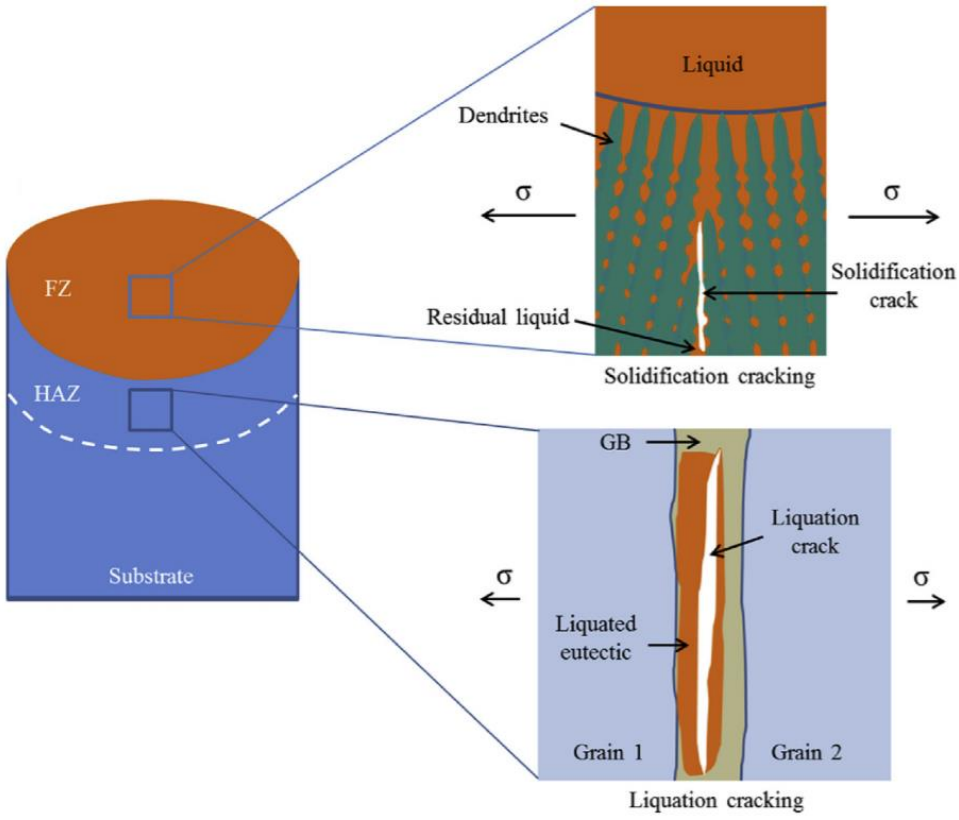

Figure 18: A schematic diagram of solidification cracking and liquation cracking which shows how the two mechanisms depend on location of formation. FZ stands for the fusion zone and HAZ stands for the heat affected zone in the image.[25]

Solidification cracking occurs at the top deposited molten layer. Microcracks form from the buildup of residual thermal stresses during AM due to the Thermal Gradient Mechanism. This means compressive stresses are introduced when the molten top layer expands but is restricted by the cooler underlayer. As this top layer solidifies, thermal contraction causes the layer to shrink and induces a bend angle towards laser, producing tensile stresses in the build direction. Layers of compressive and tensile stresses build up and microcracks form to relieve those stress.[25]

Liquation cracks form in the previously deposited underlying layers. These layers are reheated as the part is built up, which causes changes in their microstructure. Rapid heating and cooling, such as that present in DMD, results in poor diffusion of alloying elements, meaning the composition of the melt pool will vary depending on the stage of solidification. The final material to solidify becomes enriched with alloying elements, resulting in a lower melting point material. As the next layer is deposited, and the material lying in the heat affected zone is reheated, constitutional liquation occurs. This means that the low melting temperature composition melts before the bulk of the material which introduces stresses and causes liquation cracking in re-solidification.[26]

Crack characteristics differed between the three compositions tested. One explanation for these differences could be the increasing phase fraction of γ″ as Nb content increased. For example, the X2 composition had the highest amount of Nb and least amount of cracking in the microstructure. This composition also had better ductility than X1. The γ″ precipitation strengthening phase would cause a higher energy barrier for crack formation and propagation within the part. Alternatively, IN718 had many relatively small cracks compared to the X1 composition which had larger cracks. This may be because the higher γ″ phase amount in X1 could withstand more thermal stresses up to a point, but ultimately relieved those stresses in large cracks. The IN718 AM compositions had lower strength, so stresses were relieved more frequently and in random directionality than seen in the X1 or X2 compositions.

4.1.2 Dendritic Structures

Another potential reason for the low elongation were the dendritic structures found in all AM microstructures. Dendrites form from the successive stages of heat conduction from the molten zone and fast solidification. The solid-liquid interface leads to preferred growth due to the attempt of the solid to minimize surface energy, which takes place at the tips of dendrites. These dendrites could possibly be a secondary σ phase found in IN718. This phase is comprised of a tetragonal cell of 30 atoms, and usually forms after extended exposure between 540-920°C.[23] The σ phase, when present in more than trace amounts, is undesirable in nickel-based superalloys because of its brittle nature caused by directional bonding.[8] This bonding resists shearing motions during plastic deformation which results in reduced ductility. It is predicted that this phase formed during solidification and was not fully solutionized during the post-print heat treatment.

4.2 Fracture Surfaces

4.2.1 Microvoid Coalescence

The fracture surfaces of all AM samples were analyzed under the SEM (Figure 17). From the images examined, all surfaces exhibited microvoids, which nucleate at regions of localized strain discontinuities such as at precipitates, grain boundaries, and dislocation pile-ups.[27] As strain increases, microvoids grow, coalesce, and eventually form a continuous fracture surface.

It was concluded that the failure mechanism for these alloys was Microvoid Coalescence, which is a type of ductile fracture. This failure mechanism is also called “dimple rupture” because of the cup-like depressions that form from the fracturing microvoids. Microvoid Coalescence causes a ductile fracture because of debonding at particle interfaces. These interfaces are caused by inclusions or second phase particles formed in the microstructure that tend to have low-strength interface bonds between the matrix.[28] As the materials are subjected to a tensile stress, debonding occurs in the direction of maximum strain. In the case of this research, microvoids were predicted to nucleate at second-phase coherent precipitates and grain boundaries within the AM microstructure. Particles coherent within the matrix require the development of substantial

stress for decohesion to start at the particle-matrix interface. This large amount of stress required to de-bond the interface led the alloy to have higher ductility. This is a promising finding because it means the alloys have potential for higher percent elongation. The low percent elongation observed in the AM samples was likely due to microstructural defects such as microcracks and the brittle σ phase and was not necessarily a fundamental characteristic of the alloy. If these defects can be eliminated from changes in processing and heat treatment, the ductility could increase in the AM samples.

4.3 Yield Strength

4.3.1 Composition

Tensile testing showed that increasing Nb content in the AM sample compositions increased the yield strength of these alloys. The average yield strength of each composition showed an increasing trend as the phase fraction of γ″ increased, as was expected. The average wrought IN718 yield strength of 1218 MPa was higher than the AM samples of the same composition. This could be because of the presence of microcracks and the brittle σ phase in the microstructures caused this reduced strength. The X1 composition also had reduced average yield strength above one standard deviation of error compared to the wrought IN718 samples in both build directions. This could also be because of significant microcracking and dendritic structures present in the samples.

Out of all samples, the X2 alloy composition had the highest strength with 1254 MPa and 1400 MPa for the vertical and horizontal builds, respectively. These average values surpass the IN718 wrought strength above one standard deviation of error. The X2 composition's high strength is attributed to the large phase fraction of γ″ precipitates which were promoted by the high Nb content in the alloy. Despite its high strength, microstructural defects discussed above resulted in low percent elongation.

4.3.2 Directional Strength

One trend observed was that the horizontal build direction was consistently stronger than the vertical build direction. This difference could be attributed to the way samples were fabricated. Each orientation consisted of layers deposited and built up in the z-axis. For the vertical build, these layers would be perpendicular to the tensile loading axis whereas layers would be parallel to the loading axis for the horizontal build direction.

The increased horizontal strength is based on grain orientation in the layers. Unlike the wrought microstructure, AM samples have an anisotropic grain morphology. As the molten pool solidifies to form a layer, new grains nucleate and grow epitaxially from the layer below them. This means that new grains align to take on the same crystalline orientation as grains from the underlying layer. Grains oriented with their preferred growth direction parallel to the steepest thermal

gradient will solidify most rapidly, having preferential growth. In this AM process, the z-axis has the highest thermal gradient which results in columnar grains elongated in the z-axis (Figure 19).

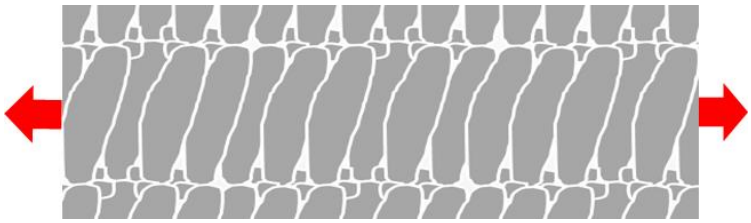

Figure 19: Schematic of the anisotropic grain morphology in the horizontal build direction. Columnar grains are elongated, resulting in a higher concentration of grain boundaries perpendicular to the loading axis. The red arrows indicate the z-axis.

Elongated anisotropic grains result in there being different concentrations of grain boundaries depending on the direction within the sample. For the horizontal build direction, the resulting microstructure had more grain boundaries perpendicular to the loading axis than found in the vertical build direction. The higher concentration of perpendicular grain boundaries inhibit dislocation motion within the material, increasing the strength of the part in the tensile loading direction.

5. Conclusions

1. Of the three compositions tested, the X2 alloy with 8.52 wt% Nb had the highest yield strength. This is due to the high Nb content which promoted the formation of coherent γ'' precipitates. The X2 composition was able to exceed the wrought IN718 yield strength.

2. Samples fabricated in the horizontal build direction during AM proved to have a higher yield strength compared to the vertical build. Print layers aligned parallel to the loading axis have a higher concentration of grain boundaries perpendicular to this axis due to their columnar structure. Grain boundaries inhibited dislocation motion strengthening the part.

3. The presence of microcracks and the brittle σ phase in AM microstructures resulted in low %EL. The coalescence of microvoids, however, signify a ductile fracture surface meaning with improved processing, these alloys have potential.

6. Works Cited

1. Bracci, Jonathon. “Overview of CalPoly AM 718 Project.” Oerlikon Metco. Oerlikon Metco, Jan. 2018.

2. AZoM, Written by. “Nickel Alloy Inconel 718 - Properties and Applications by United Performance Metals.” AZoM.com, 1 Aug. 2017.

3. Sundararaman, M., et al. “The Stability of γ′ and γ′′ Phases in Alloy 718 Under Electron Irradiation.” *Superalloys* 718. 625. 705 and Various Derivatives, 2001, pp. 379–386. TMS.

4. Bhadeshia, H.K. Nickel Based Superalloys. University of Cambridge.

5. ASM Handbook Online, D.A. DeAntonio, D. Duhl, T. Howson, and M.F. Rothman, Heat Treating of Superalloys, *Heat Treating*, Vol 4, *ASM Handbook*, ASM International, 1991, p 793–814.

6. ASM Handbooks Online, Dempster, and R. Wallis, Heat Treatment Metallurgy of Nickel-Base Alloys, *Heat Treating of Nonferrous Alloys*, Vol 4E, *ASM Handbook*, ASM International, 2016, p 399–425.

7. Mostafa, Ahmad, et al. “Erratum: Structure, Texture and Phases in 3D Printed IN718 Alloy Subjected to Homogenization and HIP Treatments. Metals 2017, 7, 196.” *Metals*, vol. 7, no. 8, 2017, p. 315.

8. Reed, Roger C. *The Superalloys: Fundamentals and Applications*. Cambridge University Press, 2008.

9. I. Dempster, and R. Wallis, Heat Treatment Metallurgy of Nickel-Base Alloys, Heat Treating of Nonferrous Alloys, Vol 4E, *ASM Handbook*, ASM International, 2016, p 399–425.

10. Choi, Hyung Sup, and Ju Choi. “Precipitation in Inconel 718 Alloy.” *Journal of the Korean Nuclear Society*, vol. 4, no. 3, Sept. 1972, pp. 203–213.

11. Schloetter, Jeffrey, et al. “Effect of Composition and Build Direction on Additively Manufactured Hastelloy X Alloys.” *California Polytechnic State University Materials Engineering Department*, 2017.

12. Dutta, B., and S. Palaniswamy. “Additive Manufacturing by Direct Metal Deposition.” *Advanced Materials & Processes*, May 2011, pp. 33–36.

13. Dinda, G.p., A.k. Dasgupta, and J. Mazumder. "Laser Aided Direct Metal Deposition of Inconel 625 Superalloy: Microstructural Evolution and Thermal Stability." *Materials Science and Engineering: A* 509.1-2 (2009): 98-104.

14. Amato, K.n., et al. “Microstructures and Mechanical Behavior of Inconel 718 Fabricated by Selective Laser Melting.” *Acta Materialia*, vol. 60, no. 5, 2012, pp. 2229–2239.

15. Chen, Hui-Chi, et al. “Fibre Laser Welding of Dissimilar Alloys of Ti-6Al-4V and Inconel 718 for Aerospace Applications.” *The International Journal of Advanced Manufacturing Technology*, vol. 52, no. 9-12, 2010, pp. 977–987.

16. Mazumder, J., et al. “Closed Loop Direct Metal Deposition: Art to Part.” *Optics and Lasers in Engineering*, vol. 34, no. 4-6, 2000, pp. 397–414.

17. Seetharaman, Sankaranarayanan, et al. “Research Updates On The Additive Manufacturing Of Nickel Based Superalloys.” Solid Freeform Fabrication , 2016.

18. CAO, PENGCHENG. “Characterization of Laser Deposited Alloy 718.” *Kth Royal Institute Of Technology School Of Industrial Engineering And Management*, 2015.

19. Harrison, Neil J., et al. “Reduction of Micro-Cracking in Nickel Superalloys Processed by Selective Laser Melting: A Fundamental Alloy Design Approach.” *Acta Materialia*, vol. 94, 2015, pp. 59–68.

20. Yang, Jingjing, et al. “Cracking Behavior and Control of Rene 104 Superalloy Produced by Direct Laser Fabrication.” Journal of Materials Processing Technology, vol. 225, 2015, pp. 229–239.

21. ASTM E8 / E8M-16a, Standard Test Methods for Tension Testing of Metallic Materials, ASTM International, West Conshohocken, PA, 2016.

22. “Safety Data Sheet Hydrochloric Acid, ACS.” *Fischer Scientific*, 8 Jan. 2015.

23. “Safety Data Sheet Cupric Chloride, Dihydrate.” *Fischer Scientific*, 21 Jan. 2015.,

24. “Safety Data Sheet Ethanol, Anhydrous.” *Fischer Scientific*, 18 Jan. 2018.

25. Xu, Jianjun, et al. “The Initiation and Propagation Mechanism of the Overlapping Zone Cracking during Laser Solid Forming of IN-738LC Superalloy.” *Journal of Alloys and Compounds*, vol. 749, 2018, pp. 859–870. Science Direct, doi:10.1016/j.jallcom.2018.03.366.

26. Chen, Yuan, et al. “Characterization of Heat Affected Zone Liquation Cracking in Laser Additive Manufacturing of Inconel 718.” Materials & Design, vol. 90, 2016, pp. 586–594. Science Direct, doi:10.1016/j.matdes.2015.10.155.

27. V. Kerlins and A. Phillips, Modes of Fracture, Fractography, Vol. 12, *ASM Handbook*, ASM International, 1987, p. 12–71.

28. W.T. Becker and D. McGarry, Mechanisms and Appearances of Ductile and Brittle Fracture in Metals, Failure Analysis and Prevention, Vol 11, *ASM Handbook*, ASM International, 2002, p 587–626.

7. Appendix

I. Standard Operating Procedures

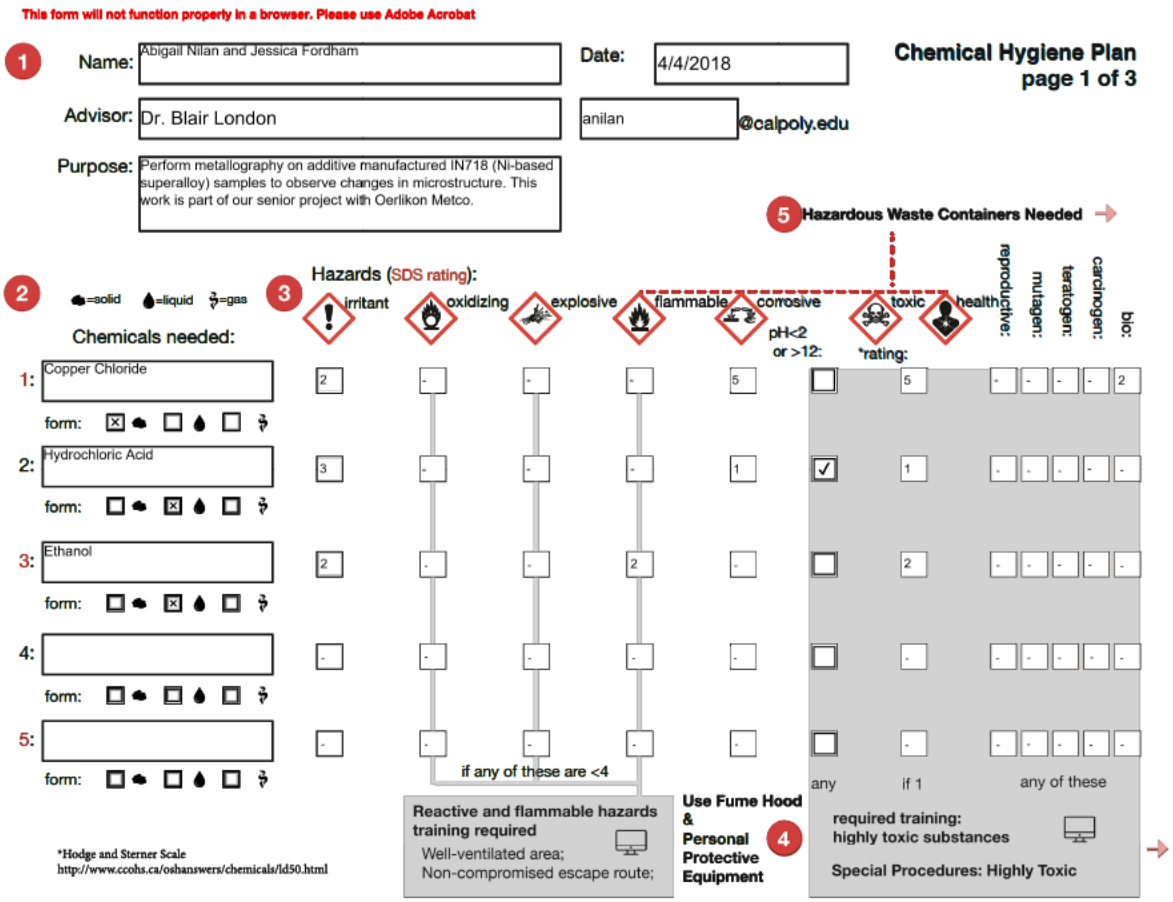

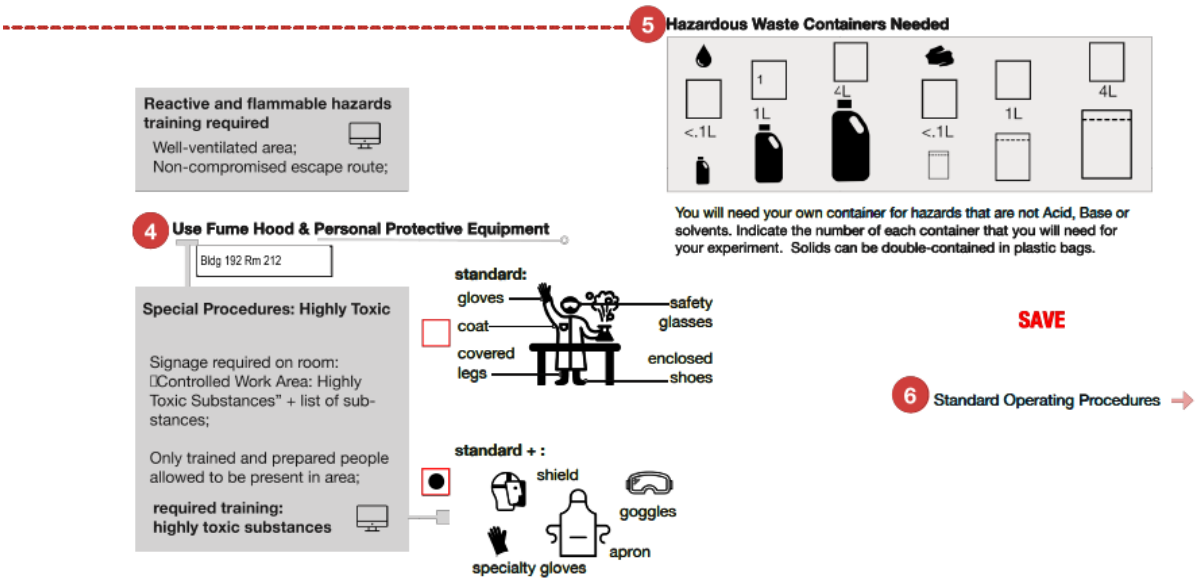
5 Hazardous Waste Containers Needed
<.1L
1L
4L
<.1L
1L
4L
You will need your own container for hazards that are not Acid, Base or solvents. Indicate the number of each container that you will need for your experiment. Solids can be double-contained in plastic bags.
Reactive and flammable hazards training required
Well-ventilated area;
Non-compromised escape route;
4 Use Fume Hood & Personal Protective Equipment
Bldg 192 Rm 212
Special Procedures: Highly Toxic
Signage required on room: "Controlled Work Area: Highly Toxic Substances" + list of substances;
Only trained and prepared people allowed to be present in area;
required training: highly toxic substances
standard:
gloves
coat
covered legs
safety glasses
enclosed shoes
standard + :
shield
goggles
apron
specialty gloves
SAVE
6 Standard Operating Procedures

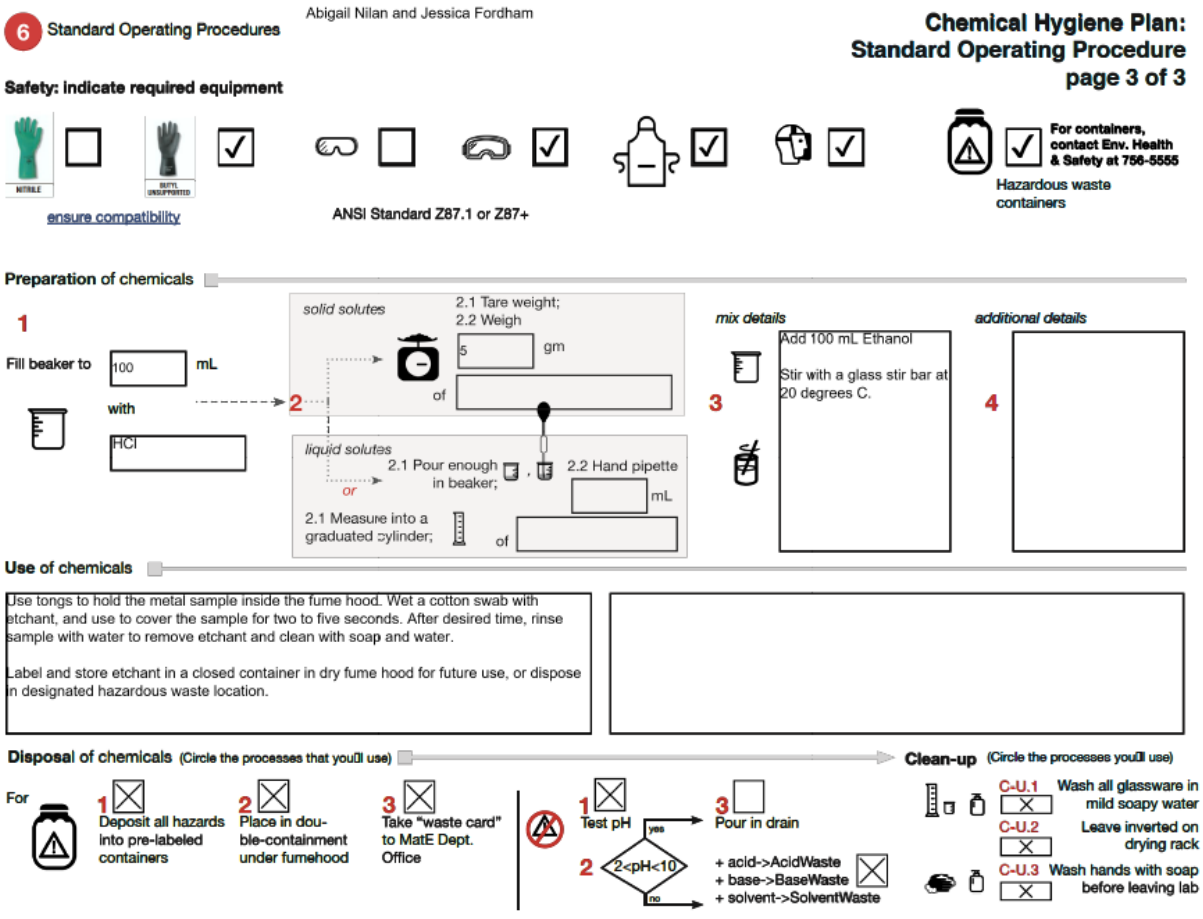
6 Standard Operating Procedures
Abigail Nilan and Jessica Fordham
Chemical Hygiene Plan:
Standard Operating Procedure
page 3 of 3
Safety: indicate required equipment
ensure compatibility
ANSI Standard Z87.1 or Z87+
For containers, contact Env. Health & Safety at 756-5555
Hazardous waste containers
Preparation of chemicals
1
Fill beaker to
100
mL
with
HCl
2
solid solutes
2.1 Tare weight;
2.2 Weigh
5
gm
of
liquid solutes
2.1 Pour enough in beaker;
or
2.1 Measure into a graduated cylinder;
2.2 Hand pipette
mL
of
mix details
3
Add 100 mL Ethanol
Stir with a glass stir bar at 20 degrees C.
additional details
4
Use of chemicals
Use tongs to hold the metal sample inside the fume hood. Wet a cotton swab with etchant, and use to cover the sample for two to five seconds. After desired time, rinse sample with water to remove etchant and clean with soap and water.
Label and store etchant in a closed container in dry fume hood for future use, or dispose in designated hazardous waste location.
Disposal of chemicals (Circle the processes that you'll use)
For
1 Deposit all hazards into pre-labeled containers
2 Place in double-containment under fumehood
3 Take "waste card" to MatE Dept. Office
1 Test pH
2 2<pH<10
yes
no
3 Pour in drain
+ acid->AcidWaste
+ base->BaseWaste
+ solvent->SolventWaste
Clean-up (Circle the processes you'll use)
C-U.1 Wash all glassware in mild soapy water
C-U.2 Leave inverted on drying rack
C-U.3 Wash hands with soap before leaving lab

II. Tensile Testing Results

Specimen ID	Young's Modulus [Gpa]	Yield Stress (0.2% Offset) [Mpa]	Maximum Load [kN]	Tensile Stress [Mpa]	% Elongation [%]
718_W_1	207.56	1224.20	27.26	1409.00	21.03
718_W_2	205.87	1216.00	27.22	1397.60	20.97
718_W_3	215.25	1214.00	27.24	1410.00	20.45
718_V_1	153.96	381.10	10.87	481.60	8.36
718_V_2	152.62	361.60	9.94	439.70	5.50
718_V_3	163.93	382.30	11.83	523.70	13.06
718_H_1	142.87	1036.40	22.78	1087.70	1.48
718_H_2	134.67	908.00	20.86	993.10	1.72
718_H_3	148.58	1057.00	24.78	1188.80	4.50
718X1_V_1	197.22	963.10	23.44	1003.40	0.92
718X1_V_2	174.72	991.70	22.39	1016.60	.82?
718X1_V_3	155.83	946.50	22.67	969.80	1.02
718X1_H_1	162.77	1180.30	26.56	1281.70	1.83
718X1_H_2	145.66	1004.80	20.89	1021.10	0.90
718X1_H_3	168.68	1146.70	25.64	1259.40	1.51
718X2_V_1	245.65	1224.70	37.59	1449.20	2.29
718X2_V_2	198.42	1289.50	35.61	1377.60	1.28
718X2_V_3	194.96	1247.50	35.97	1390.20	2.25
718X2_H_1	220.13	1377.90	32.81	1510.50	1.87
718X2_H_2	195.98	1408.60	33.41	1532.50	2.26
718X2_H_3	189.46	1413.10	33.40	1536.10	2.35

III. X2 and X1 Tensile Curves

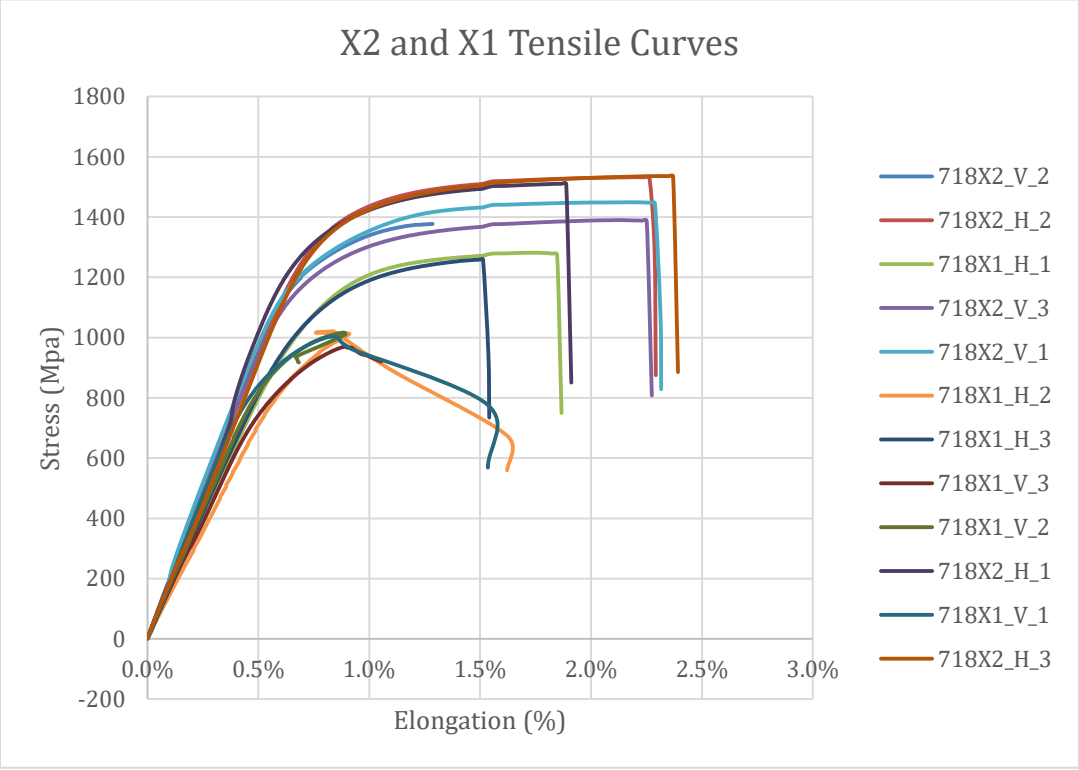

IV. 718 Wrought and AM Tensile Curves